NACA

RESEARCH MEMORANDUM

A TRANSONIC INVESTIGATION BY THE FREE-FALL METHOD OF AN

AIRPLANE CONFIGURATION HAVING 45° SWEPTBACK

WING AND TAIL SURFACES

By Stanley Faber and John M. Eggleston

Langley Aeronautical Laboratory
Langley Field, Va.

NATIONAL ADVISORY COMMITTEE
FOR AERONAUTICS
WASHINGTON
June 11, 1953

NACA RM L53D10

NATIONAL ADVISORY COMMITTEE FOR AERONAUTICS

RESEARCH MEMORANDUM

A TRANSONIC INVESTIGATION BY THE FREE-FALL METHOD OF AN

AIRPLANE CONFIGURATION HAVING 45° SWEPTBACK

WING AND TAIL SURFACES

By Stanley Faber and John M. Eggleston

SUMMARY

As part of a general investigation to obtain the characteristics of airplanes in the transonic range, the Langley Laboratory, by using the free-fall technique, has tested an airplane configuration having 45° sweptback wing and tail surfaces. The model was equipped with an all-movable horizontal tail that was stepped cyclically during the drop to vary the angle of attack. In this manner, the lift, drag, and longitudinal static and dynamic stability and control characteristics were obtained at various operating lift coefficients up to 0.26 over a Mach number range of 0.5 to 1.21. The Reynolds number range was from 2.5×10^6 at release to 16.0×10^6 at impact. Comparisons were made with test results of aerodynamically similar models of other transonic facilities in order that correlation between these facilities can be obtained.

The results of free-fall tests showed that only small trim changes in angle of attack and trim lift coefficient were experienced at high subsonic speeds. The lift-curve slope increased with increasing Mach number up to a Mach number of 0.97 and thereafter decreased.

At Mach numbers near 1.2, the drag results indicate that some leading-edge suction was realized but that it was only a moderate percentage of the amount predicted by theory.

The ability of the horizontal tail to change the lift coefficient increased with increases in Mach number up to Mach number 0.9 and thereafter decreased. At the highest Mach number of the test, the tail was only half as effective in changing the trim lift coefficient as it was at low subsonic speeds. The model experienced a large increase in stability at a Mach number of 0.9; the aerodynamic-center position moved from 40 percent of the mean aerodynamic chord rapidly rearward until at a Mach number of 1.17 the aerodynamic center was at 70 percent of the mean aerodynamic chord.

The longitudinal damping derivatives of the model indicated an
increase in damping with increasing Mach number in the subsonic region
and a more pronounced decrease in damping with increasing Mach number
supersonically.

The stability parameters as calculated from the wind-tunnel data
for purposes of comparison indicated the same general trends as the
free-fall results. The most pronounced difference was in the Mach num-
ber at which the large increase in static stability begins; the wind-
tunnel results predicted this increase at a Mach number of approximately
0.1 earlier than the free-fall results. Estimations of aeroelastic
effects indicate that such effects were not a factor in these comparisons.

INTRODUCTION

As part of a general investigation to obtain the characteristics
of airplanes in the transonic range, the Langley Laboratory, by using
the free-fall technique, has tested an airplane configuration having
45° sweptback wing and tail surfaces. The all-movable horizontal tail
of this model was stepped cyclically in small increments during the
drop in order to vary the angle of attack. In this manner, the transonic
lift and drag, and the longitudinal static and dynamic stability and
control characteristics were obtained at various operating lift coef-
ficients (up to a value of 0.26) and over a Mach number range of 0.5
to 1.21. The Reynolds number range was from 2.5×10^{6} at release to
16.0×10^{6} at impact.

Directly comparable tests of aerodynamically similar models are
being made by several other transonic facilities of the Langley
Laboratory in order that correlation between transonic testing techniques
can be obtained.

The results of the free-fall test are presented herein as the vari-
ation with Mach number of the lift coefficient, drag coefficient, lift-
curve slope, pitching-moment slope, and damping-in-pitch derivatives.
These results are compared with the parameters estimated from the tran-
sonic wind-tunnel tests of the same wing-fuselage combination as reported
in references 1 to 4 and with the zero-lift drag for the wing-fuselage
combination as obtained from previous free-fall tests (ref. 5). Frequency-
response curves are also presented as obtained from the response of the
model in angle of attack and normal acceleration to the step elevator
deflections.

SYMBOLS

a exponential damping factor, as in e^{at}, negative for stable oscillation, sec^{-1}

$\bar{c}$ mean aerodynamic chord, ft

C_c chord force coefficient, rW/qS

C_L lift coefficient, $C_N \cos \alpha - C_c \sin \alpha$

ΔC_L incremental change in lift coefficient

C_D drag coefficient, $C_N \sin \alpha + C_c \cos \alpha$

C_m pitching-moment coefficient, $M/qS\bar{c}$

C_N normal-force coefficient, nW/qS

C_{L_α} variation of lift coefficient with angle of attack, per deg

$C_{L_{i_t}}$ variation of lift coefficient with tail incidence, per deg

C_{m_α} variation of pitching-moment coefficient with angle of attack, per deg

$C_{m_{i_t}}$ variation of pitching-moment coefficient with tail incidence, per deg

C_{m_q} variation of pitching-moment coefficient with pitching velocity (nondimensional), $\partial C_m \big/ \partial \dfrac{\dot{\theta}\bar{c}}{2V}$

$C_{m_{D_\alpha}}$ variation of pitching-moment coefficient with rate of change of angle of attack (nondimensional), $\partial C_m \big/ \partial \dfrac{\dot{\alpha}\bar{c}}{2V}$

D differential operator, $\dfrac{\bar{c}}{V}\dfrac{d}{dt}$

f frequency, cycles/sec

g	acceleration of gravity, ft/sec^2
I_y	moment of inertia about lateral axis, slug-ft^2
i_t	tail incidence, deg
Δi_t	incremental change in tail incidence, deg
K_y	nondimensional radius of gyration, $I/m\bar{c}^2$
l	tail length, ft
l_1	distance from angle-of-attack vane to center of gravity, ft
l_2	distance from normal accelerometer to center of gravity, ft
m	mass, slugs
M	Mach number; or pitching moment, ft-lb
n	normal acceleration in g units
p	static pressure, lb/sq ft
q	dynamic pressure, $\frac{\gamma}{2}pM^2$, lb/sq ft
r	longitudinal retardation in g units
S	wing area, sq ft
S_t	tail area, sq ft
s	LaPlace transform operator
t	time, sec
V	velocity, ft/sec
α	angle of attack, deg
$\Delta\alpha$	incremental change in angle of attack, deg
$\dot{\alpha}$	rate of change of angle of attack, radians/sec
γ	ratio of specific heats, 1.4 for air

$\dot{\theta}$ pitching velocity, radians/sec

$\ddot{\theta}$ pitching acceleration, radians/sec^2

$d\epsilon/d\alpha$ variation of downwash angle with angle of attack

μ airplane relative-density factor, $m/\rho S\bar{c}$

ρ density, slugs/cu ft

Subscripts:

f   fuselage

t   tail

w   wing

    The systems of axes used in this report with positive directions and deflections are shown in figure 1. In plotting the frequency-response data, the sign of the tail incidence has been reversed to agree with dynamic-analysis conventions.

MODEL

    The test model was a midwing airplane configuration as shown in the photograph in figure 2. A drawing of the model giving the pertinent dimensions is presented as figure 3.

    The fuselage had a fineness ratio of 10, obtained by cutting off the rear one-sixth of a fineness-ratio-12 body. Table I gives the coordinates of the body. Reference 6 contains results of drop tests of the body alone. The wing of the model had 45° of sweepback measured at the quarter-chord line, an aspect ratio of 4, a taper ratio of 0.6, and an NACA 65A006 airfoil section parallel to the plane of symmetry. The wing had no dihedral or incidence and was located on the body such that the quarter chord of the mean aerodynamic chord was at 60 percent of the body length, the approximate model center of gravity. The all-movable horizontal tail was scaled down from the wing, the linear ratio being 0.448, and was mounted in a slot in the vertical fin 26.4 percent of the wing semispan above the wing-chord plane. The pivot point of the tail was at a chordwise location of approximately 29 percent of the horizontal-tail mean aerodynamic chord. The slot in the vertical tail was sealed by cover plates attached to the horizontal tail. In order to keep the cover plates from blowing out, small shrouds were placed over the leading edge of the cover plates and were attached to the fin.

The juncture of the tail surfaces incorporated a large rectangular
fairing used primarily to provide the horizontal tail with adequate
rigidity. The fairing also provided a flat surface for more effective
sealing action of the cover plates. The fin had an NACA 65A009 airfoil
section parallel to the body center line, an aspect ratio of 1.5, a
taper ratio of 0.5 and had the trailing edge swept back 45°. A photo-
graph of the tail is shown in figure 4.

In order to obtain high strength and stiffness, the wing was made
with a core of heat-treated steel. This core was covered with bismuth-
tin alloy to form the actual airfoil shape. The vertical and horizontal
tails were machined from solid aluminum.

The alinement of the model was very carefully controlled during
construction in order to keep the rate of roll low. The necessity for
keeping the rate of roll low stems from the desire of keeping the effects
of rolling on the model stability small, as discussed in reference 7.
Ground measurements showed the wing to have zero twist and an incidence
angle of less than 1 minute. The vertical tail had a slight twist of
about 4 minutes over its span, which was estimated to produce a rate of
roll of one revolution per minute.

The model weighed 1030 pounds with the center of gravity at 23.64 per-
cent of the wing mean aerodynamic chord. The loading of the model was
heavily concentrated near the model center of gravity in order to reduce
any gyroscopic and centrifugal moments that would be produced by rolling.
The moment of inertia of the model about the lateral axis through the
center of gravity was 50.1 slug-ft^2 and the wing loading was 114.5 lb/sq ft.

The incidence of the horizontal tail was changed during the drop in
small increments by a stepping cam which was designed to give 2 seconds
of fixed incidence at each position. The measured incidence angles were
1.15°, 0.32°, -0.12°, -0.60°, -1.12°, -1.58°, -2.07°, and -2.87°. A
time delay was employed to prevent the tail mechanism from operating
during the initial 15 seconds so that the model could increase in speed
at essentially zero lift and so that the model would not be at high lift
coefficients near a Mach number of 0.9. Preliminary investigations
showed the longitudinal stability to be marginal at this Mach number.

MEASUREMENTS

The test was performed by utilizing the free-fall method in which
the flight path of the freely falling test body is obtained by radar and
phototheodolite equipment and the other desired quantities are measured
at the model by means of the NACA radio-telemetering system. References 5
and 6 contain more complete details of this technique. An atmospheric

survey of static pressure, temperature, and wind direction and velocity was made after the drop. The quantities measured and recorded by the telemetering system were: longitudinal retardation, normal acceleration, and transverse acceleration, all by accelerometers located 22 inches ahead of the center of gravity; the angle of attack, by a delta-shaped vane 7 inches ahead of the model nose (see fig. 5); the tail deflection, at the root of the horizontal tail; the ambient pressure, inside the base of the conical body of the angle-of-attack vane; the impact pressure, by a probe located 5 inches back from the body nose and 1 inch from the body surface (see fig. 5); and the rate of roll, by a rate gyro mounted in the model nose.

The quantities which were used to determine the Mach number during the drop are presented as time histories in figure 6. The Mach number was obtained by first differentiating the flight path with respect to time to obtain the velocity of the model relative to the ground. This velocity was combined with the wind velocity to obtain the true airspeed. The Mach number was then determined from the true airspeed and the atmospheric temperature. The Mach number could be obtained from the radar-phototheodolite data for all but the last portion of the drop; a ground haze obscured the model from the optical trackers after 46 seconds from release. An auxiliary measurement of the Mach number was obtained from the telemetered impact pressure and the survey static pressure. These data were used to extrapolate the Mach number variation to impact as shown in figure 6. The Mach number variation thus obtained is believed to be accurate to within ± 0.01.

REDUCTION OF DATA

The acceleration and retardation data were reduced to normal- and chord-force coefficients by using the model weight and wing area and the appropriate Mach number and static pressure. Lift and drag coefficients C_L and C_D were obtained from the normal- and chord-force coefficients and the measured angle of attack. The variation of lift coefficient with angle of attack was obtained from incremental changes in the trim value of the parameters C_L and α at each stabilizer step. These values were corrected to the case of constant tail incidence through use of the formula

$$C_{L_\alpha} = \frac{\Delta C_L}{\Delta \alpha} - \frac{S_T}{S} \frac{\Delta i_t}{\Delta \alpha} C_{L_{\alpha_t}}$$

where $\Delta i_t / \Delta\alpha$ is the change in tail incidence divided by the change in the trim value of the angle of attack. The tail lift-curve slope was estimated from tunnel tests of the wing inasmuch as the wing and tail of the model were geometrically similar. The effects of aeroelasticity on the lift-curve slope of the tail of the free-fall model were found to be about the same as those for the wing used in the wind-tunnel tests. Therefore, no corrections for aeroelasticity were made.

Corrected values of the lift-curve slope were also obtained from the alternate formula

$$C_{L_\alpha} = \frac{\dfrac{\Delta C_L}{\Delta\alpha}\left[1 + \dfrac{S_T}{S}\left(1 - \dfrac{d\epsilon}{d\alpha}\right)\right]}{1 + \dfrac{S_T}{S}\left(1 - \dfrac{d\epsilon}{d\alpha} + \dfrac{\Delta i_t}{\Delta\alpha}\right)}$$

The derivation of this equation assumes the lift-curve slope of the wing and of the tail to be the same. Somewhat different values of the lift-curve slopes would be expected because of the effects of aeroelasticity as the wing and tail were made of different materials; however, as will be shown subsequently, this effect of aeroelasticity is small and consideration of such effects in the formula does not significantly change the final result. Downwash values for this correction and for all calculations in this report were obtained from wind-tunnel data of reference 4 for the tail location of the free-fall model. The two methods used to correct the model lift-curve slope gave essentially the same results.

The rigid-wing lift-curve slopes were obtained by correcting the measured $C_{L_{\alpha_W}}$ by the methods of reference 8 as applied to a solid wing. Reference 9 was also used to obtain the rigid wing $C_{L_{\alpha_W}}$ and gave results in good agreement with those of reference 8.

The zero-lift drag coefficient at supersonic speeds was obtained from the formula

$$C_{D_{C_L=0}} = C_D - \frac{C_L^2}{57.3 C_{L_\alpha}}$$

This formula applies when no leading-edge suction is present. The zero-lift drag coefficient was also estimated at $M = 1.2$ by using the test

data obtained in the Mach range 1.17 to 1.21. In this Mach number range dC_D/dC_L^2 was found to be 0.216.

The variation of the pitching-moment coefficient with angle of attack C_{m_α} was calculated by use of the equation

$$C_{m_\alpha} = \frac{-(2\pi f)^2 I_y}{q S \bar{c}}$$

The effects on the frequency of the damping in pitch and the degree of freedom involving motion along the vertical axis were neglected because these effects were found negligible for this model.

The damping coefficients $C_{m_{D_\alpha}} + C_{m_q}$ were calculated from the formula

$$C_{m_{D_\alpha}} + C_{m_q} = \frac{2I_y}{m\bar{c}^2} C_{L_\alpha} + \frac{4I_y a V}{q S \bar{c}^2}$$

where V is the true airspeed, and a is the damping exponent. The derivation of the equation for the damping coefficients was based on the assumptions that the model had two degrees of freedom.

The estimated maximum uncertainties of the basic coefficients obtained from the telemetered measurements are presented in the following table for two Mach numbers. The uncertainties are based on an instrument error of ±1 percent of the instrument range.

M	C_L	C_D	C_{m_α}
0.8	±0.029	±0.0082	±0.0010
1.2	±.010	±.0027	±.0013

The maximum uncertainties of other pertinent quantities that do not vary with Mach number are as follows:

Angle of attack, deg . . . .   ±0.15
Tail incidence (measured at root), deg . . . .   ±0.02
Rate of roll, radians/sec . . . .   ±0.02
Transverse acceleration, g units . . . .   ±0.02

The measured response of the model to the step elevator deflections were analyzed by using the Prony method to obtain the transfer functions in angle of attack and normal acceleration. The Prony method is described in reference 10 and, in brief, this method of analysis assumes that the control input and transient response may be expressed by a series of exponentials. The coefficients of the resulting analytical expressions are solved by a least-squares method, and the transfer function is then established by taking the LaPlace transform of these analytical expressions. Transfer functions were obtained from the response in angle of attack as recorded at a point 5.5 feet (l_1) ahead of the center of gravity and from the response in normal acceleration as measured at a point 2.165 feet (l_2) ahead of the center of gravity. With these transfer functions, the following relationships were solved simultaneously to establish the transfer functions in angle of attack and normal acceleration at the center of gravity.

$$\left[\frac{\alpha}{i_t}\right]_{cg} = \left[\frac{\alpha}{i_t}\right] + \frac{l_1}{V}\left[\frac{\dot{\theta}}{i_t}\right]$$

$$\left[\frac{n_\theta}{i_t}\right]_{cg} = \left[\frac{n}{i_t}\right] - \frac{l_2}{g}\left[\frac{\ddot{\theta}}{i_t}\right]$$

$$\left[\frac{\dot{\theta}}{i_t}\right]_{cg} = \left[\frac{\dot{\alpha}}{i_t}\right]_{cg} + \frac{g}{V}\left[\frac{n}{i_t}\right]_{cg}$$

These equations are based on the system of axes shown in figure 1.

RESULTS AND DISCUSSION

General.- A full-size reproduction of a section of the telemeter
record is shown in figure 7. The high-frequency oscillation (approxi-
mately 47 cps) in the normal acceleration following the step is the
first bending mode of the horizontal tail. Since the tail is swept back
this bending produces oscillating tail loads which are reflected in the
normal acceleration. The recorded amplitude of the oscillation is
exaggerated somewhat by the accelerometer being located ahead of the
center of gravity where it is sensitive to pitching accelerations. For
the calculations based on these data this oscillation was faired.

Complete time histories of the basic measurements obtained from
the test are presented in figure 8. The figure shows that the time
delay in the tail-programming device operated to produce the desired
15-second time delay before the first step in control deflection occurred.
The Mach number obtained at the time of this first step was 0.7. The
programmer completed two cycles during the drop. At 4 seconds before
impact, the activating mechanism became jammed during the return stroke
that finishes the cycle. This jamming was probably due to the hinge
moments of the tail exceeding the output of the driving mechanism. The
rate of roll can be seen to be small throughout the drop so that its
effect on the stability of the model can be neglected. The transverse
acceleration also was small; the small residual oscillation in the trans-
verse acceleration which persisted throughout the drop is evidence that
the configuration has some snaking tendencies. If a side-force coef-
ficient of 0.01 per degree is assumed, the snaking oscillation had a
fairly constant double amplitude of one-fifth of a degree.

Lift characteristics.- The value of lift coefficient existing during
the drop is shown in figure 9 with the corresponding incidence angles of
the tail indicated. Because these lift coefficients were measured by an
accelerometer located ahead of the center of gravity, the peak values of
lift coefficient are affected by pitching acceleration. The oscillations
shown were faired over small ranges of Mach number to obtain the average
lift coefficient for a given tail incidence and Mach number. It should
be remembered that variations with Mach number of the parameters presented
herein should be associated with the particular trim lift coefficient
which existed at each test Mach number. Examination of figure 9 shows
quite clearly the effect of Mach number on the trim lift coefficients.
Up to a Mach number of 0.91, Mach number has little effect on the trim C_L
for a given tail incidence but, above this value, the trim C_L decreases
with increasing Mach number until a Mach number of 0.98, at which time a
sharp increase in trim C_L occurs. An increase in trim C_L with
increasing Mach number is also indicated in the Mach number range 1.125
to 1.15. The maximum lift coefficients reached were 0.26 in the Mach num-
ber range of 1.03 to 1.08 and 0.255 in the Mach number range of 1.165 to 1.185.

The lift-curve slope of the complete model C_{L_α} is shown in figure 10 and is compared with the C_{L_α} calculated from the wind-tunnel tests of references 1 to 4 and in the subsonic region with the theoretical C_{L_α} from reference 11. Also shown are the lift-curve slopes of the equivalent rigid wings. The lift-curve slopes were taken at the value of the mean lift coefficient existing at each test Mach number. The lift-curve slopes for the wing-body alone from the wind-tunnel data were corrected to the complete airplane configuration through use of the expression

$$C_{L_\alpha} = C_{L_{\alpha_{w+f}}}\left[1 + \frac{S_T}{S}\left(1 - \frac{d\epsilon}{d\alpha}\right)\right]$$

The theoretical wing lift-curve slope was corrected to the complete airplane lift-curve slope by the same expression. The values of C_{L_α} determined from the free-fall test increased from the subsonic value of 0.07 to a maximum of 0.108 at approximately $M = 0.97$ and then decreased to a value of 0.07 at $M = 1.2$. At subsonic speeds the variation of C_{L_α} obtained from the wind-tunnel tests has the same general shape as from the free-fall test, but the values from the wind-tunnel tests are smaller by a fairly constant amount of 0.005. In the high subsonic range, the tunnel C_{L_α} does not peak as sharply as was indicated by the free-fall tests. As the Mach number is increased above unity, the decrease in the tunnel C_{L_α} is not so great as that shown by the present test, the tunnel value eventually becoming greater than free-fall value at the highest test Mach numbers. The theoretical curve has the same values as the wind-tunnel results for Mach numbers below 0.8 but does not indicate the sharp increase with increasing Mach number that both the free-fall and the wind-tunnel results show.

In order to investigate the effects of aeroelasticity on the comparison of the free-fall and wind-tunnel results, the lift-curve slopes for the rigid wing were calculated by using the methods of reference 8. For the free-fall data, the wing stiffness was based on that of the steel core of the model wing. For the tunnel data, reference 3 shows that, in the range of lift coefficients of the present tests, no measurable differences in lift coefficient were found between a steel and an aluminum wing. The steel wing was used for calculating aeroelastic effects on the wind-tunnel data. Correcting for the effects of aeroelasticity of the free-fall model tended to increase the value of the rigid-wing lift-curve slope over that of the flexible wing. The magnitude of this effect increased throughout the drop primarily because of the associated increase in dynamic pressure. The increase in lift-curve slope was negligible at $M = 0.5$ and increased

to about 16 percent at $M = 1.2$. The wind-tunnel tests, with a smaller variation in dynamic pressure, show an increase in rigid-wing lift-curve slope over that for the flexible wing ranging from 2 percent at low Mach numbers to 8 percent near the speed of sound and 7 percent at the highest Mach numbers. The comparison of the two models on the basis of rigid-wing lift-curve slope gives the same general conclusions as were shown by the measured results.

Drag characteristics.- The variation of the drag coefficient C_D with Mach number is shown in figure 11. Also shown in the figure is a fairing of the zero-lift drag coefficient of the model at supersonic speeds estimated from the test data by using a lift-drag variation inversely proportional to the lift-curve slope. The zero-lift drag coefficient was also obtained at $M = 1.2$ through use of the lift-drag polar established from the test data in the Mach number range 1.17 to 1.21 and also through use of the methods of reference 12. As a basis for comparison, wind-tunnel drag coefficients corresponding to the mean lift coefficients at each stabilizer step of the present test and free-fall zero-lift drag from reference 5 are shown, both sets of data having been adjusted for the differences in configuration. For the wind-tunnel data, this adjustment involved addition of the estimated drags of the horizontal and vertical tails, correction of the base pressure drag, and correction for the sting error. Adjustments to the zero-lift drag of reference 5 included addition of the drags of the vertical and horizontal tail and correction for the difference in afterbody shape. Because of the differences in instrumentation the drag coefficients of the present test are only one-third as accurate as those of reference 5.

Figure 11 shows that, in general, the drag coefficients of all the tests are in good agreement. In the high subsonic range, the wind-tunnel results indicate an earlier drag rise, but the differences are within the estimated uncertainties in Mach number. At supersonic speeds, the results of reference 5 indicate a gradual increase in zero-lift drag coefficient with increasing Mach number. The estimated zero-lift drag coefficient of the present test also shows an increase but of a much reduced magnitude. From figure 9, it can be seen that in a number of instances the operating lift coefficient was nearly the same over two ranges of Mach number. Comparison of the corresponding drag coefficients in figure 11 indicates that, under lifting conditions, there is an increase in drag coefficient with increases in Mach number. The rate of increase thus obtained is compatible with that of reference 5.

The zero-lift drag coefficient at $M = 1.2$ obtained by extrapolation of the measured lift-drag polar lies between the value estimated through use of the relationship involving the inverse of the lift-curve slope (no leading-edge suction) and the values estimated through use of reference 12 (full leading-edge suction). The position of the value obtained from the lift-drag polar indicates that some leading-edge suction was realized but only a moderate percentage of the full theoretical amount.

Control characteristics.- The ability of the tail to change the model trim lift coefficient, plotted as $\Delta C_L/\Delta i_t$, is shown in figure 12. The parameter increases from a subsonic value of 0.092 to a maximum of 0.126 at $M = 0.9$ and then decreases to a value of 0.045 at $M = 1.2$. The first part of the decrease, that just after $M = 0.9$, was due to a gradual increase in the stability of the model due to the rearward shift of the aerodynamic center of the wing-body combination. Further decreases up to the maximum Mach number of the test were due in part to this cause and in part to the decreases in the lift-curve slopes of the wing and tail as indicated by figure 10.

The variation of model lift coefficient with tail incidence is shown in figure 13 for a Mach number of approximately 1.2. The variation is shown to be fairly linear and shows that the trends in $\Delta C_L/\Delta i_t$ discussed above are not affected by lift coefficient in the range of lift coefficients of this test. This nearly linear variation of $\Delta C_L/\Delta i_t$ also validates the use of the parameter $di_t/d\alpha$ in the equation for determining the lift-curve slope.

Static stability characteristics.- From the angle of attack and the normal acceleration records (see fig. 7), the frequency of the oscillation following the step inputs were obtained. Figure 14 shows these data converted to the variation in pitching-moment coefficient with angle of attack C_{m_α} about the model center of gravity. Also shown is C_{m_α} calculated from the wind-tunnel results, which was obtained by adding the experimental C_{m_α} for the wing plus fuselage at the test C_L, corrected to the model center-of-gravity location, to the estimated C_{m_α} contribution from the tail. The tail contribution was obtained from the expression

$$\left(C_{m_\alpha}\right)_t = \left(C_{L_\alpha}\right)_w\left(1 - \frac{d\epsilon}{d\alpha}\right)\frac{S_T}{S}\frac{l}{\bar{c}}$$

Also presented in figure 14 are the values of C_{m_α} obtained from both the free-fall and the wind-tunnel models corrected for the effects of aeroelasticity by the methods of reference 8. In the subsonic region, the C_{m_α} of the free-fall model had a slight variation around a mean value of -0.016 up to $M = 0.9$, where there was a stable break, C_{m_α} reaching a maximum of -0.0395 at $M = 1.13$. The stability then decreases to a value of approximately -0.032 at $M = 1.2$. The values estimated from the wind-tunnel tests are in fair agreement with those of the present

test with the exception that the stable break in the pitching-moment curve occurs at roughly 0.1M earlier in the case of the wind-tunnel test. Slotted-throat data (ref. 2) were used to obtain the wind-tunnel value of C_{m_α}; however, the closed-throat data (ref. 1) would give essentially the same Mach number of the pitching-moment break. The data corrected to the rigid configuration show the same results as did the data of the flexible models, the value of C_{m_α} for the rigid case being only slightly more stable than C_{m_α} for the flexible case by an amount roughly proportional to the dynamic pressure.

Figure 15 shows the variation of the aerodynamic-center position with Mach number of the complete configuration; again, a comparison is made with the wind-tunnel estimates. Also shown is the aerodynamic-center position of the rigid configuration. Subsonically, the aerodynamic-center position tends to move forward with increasing Mach number from 48 percent mean aerodynamic chord to 41 percent mean aerodynamic chord at $M = 0.9$ and thereafter the configuration becomes increasingly more stable; the aerodynamic-center position reaching a value of approximately 70 percent mean aerodynamic chord at $M = 1.17$. The wind-tunnel data agreed with the test data at low Mach numbers and at $M = 1.2$. In the transonic range, the wind-tunnel data indicated a more rearward location of the aerodynamic center than did the free-fall data.

The effects of aeroelasticity shown in figure 15 for the case of the free-fall model resulted primarily from a greater reduction in the lift-curve slope of the tail than of the wing; this effect was due to the difference in material used for these components. This factor did not contribute to the effects of aeroelasticity calculated for the wind-tunnel results since the tail was assumed to be of the same material as the wing. The other factor which affects the shift in model aerodynamic-center position due to aeroelasticity is the shift in the aerodynamic center of the wing itself. This factor was estimated to be small for both models. The over-all effect on the free-fall model was that the rigid model would have a more rearward location of the aerodynamic center from that of the flexible model, the displacement being roughly proportional to the dynamic pressure.

Damping characteristics.- The damping of the model, shown in coefficient form $C_{m_q} + C_{m_{D\alpha}}$ is presented in figure 16. The data have wide scatter due to the relatively small amplitude of the pitch oscillations. These small amplitudes were difficult to measure and also showed, in some instances, evidences of nonlinear damping characteristics. The general trend of the data indicated that the damping increased as the Mach number was increased to unity and thereafter decreased with further increases in Mach number. The damping in the transonic region was approximately 50 percent greater than the damping at the low- and high-speed ends

of the test curve, $M = 0.5$ and 1.2. The data shown in figure 16 for comparison were calculated from the wind-tunnel results by assuming all the damping to be contributed by the horizontal tail. This damping was obtained from the expression

$$C_{m_q} + C_{m_{D\alpha}} = 2C_{L\alpha_W}\left(1 + \frac{d\epsilon}{d\alpha}\right)\frac{l^2}{\bar{c}^2}\frac{S_t}{S}$$

The estimates thus obtained are generally smaller than those for the free-fall data and any discrepancy may be due in part to the damping supplied by the wing-body combination.

In order to evaluate the period and damping of the test airplane configuration with respect to the current handling-qualities specifications (ref. 13), the aerodynamic derivatives of the present test were used to calculate the dynamic characteristics of a full-size fighter airplane flying at 30,000 feet. Values for the example airplane of the quantities affecting the damping are typical of current design practices. These values are as follows: wing loading of 65 lb/ft^2, moment of inertia in pitch of 23,600 slug-ft^2, and a wing span of 30 ft. As compared with the model constants, the wing loading was halved, the radius of gyration was increased by a factor of approximately 7, and the size was increased by a factor of 5. The calculations were made for the center-of-gravity position of the test model and for a center-of-gravity position that would give a minimum subsonic static margin of 5 percent of the mean aerodynamic chord. These results are shown in figure 17 plotted as the cycles to damp to 1/10 amplitude. The specification states that the oscillation shall damp to 1/10 amplitude in one cycle. The data in figure 17 show that for the rearward center-of-gravity location the specification is met for all Mach numbers below unity, the cycles required being just less than one in the low subsonic range, 6/10 of a cycle at a Mach number of 0.9, and thereafter increasing to $2\frac{1}{10}$ cycles at $M = 1.2$. For the model center-of-gravity location the curve was displaced such that only near $M = 0.9$ was the specification approximated, the airplane requiring $1\frac{1}{2}$ cycles to damp to 1/10 amplitude subsonically and $2\frac{1}{2}$ cycles at $M = 1.2$. A fact of interest here is that present experience indicates the specification may be too severe. Many current airplanes do not meet this requirement at high altitudes.

Frequency-response characteristics.- The foregoing discussion of period and damping characteristics of the test model describes its free motions. In order to further describe the dynamic characteristics of

the model in response to elevator inputs, the frequency response and
associated transfer functions have been calculated from the test data.
With the model considered to be a linear system at any one condition
of altitude, Mach number, and so forth, the frequency response in angle
of attack and normal acceleration at the center of gravity to horizontal-
tail movement was obtained by using the Prony method of analysis (ref. 10)
and assuming two degrees of freedom. These frequency responses at given
values of Mach number and over a pertinent range of frequencies are pre-
sented in figure 18 for angle of attack and in figure 19 for normal acceler-
ation. The transfer functions, which describe the inherent dynamic charac-
teristics of the model in response to an arbitrary input are presented in
table II together with the flight conditions at which they were obtained.
The transfer functions may be derived from the longitudinal equations
given in reference 14. Although the freely falling body was not kept at
a constant Mach number or altitude, the records were analyzed over periods
short enough so that it appeared justifiable to average changes in alti-
tude and Mach number. Nevertheless, the records were long enough to give
reasonable accuracy in analysis. The procedure used for obtaining the
transfer functions was such as to compensate for the effects of initial
conditions.

Examination of figures 18 and 19 shows that the frequency at which
the peaks in amplitude ratio occur increased with increasing Mach number.
This is the trend expected for the usual subsonic airplane. The high
peak values of amplitude ratio relative to their static values is indi-
cative of the low damping of the model. At these low values of damping
the natural frequency of the model may be considered to be nearly equal
to the frequency at which these peaks in the amplitude ratio occur.

Since, for the free-fall model, increasing Mach number was obtained
at decreasing altitude, the effect of altitude cannot be completely
separated from the effect of Mach number. It should be expected, however,
that damping would increase with decreasing altitude. (This effect would
be indicated by a reduction in peak amplitude ratio relative to the static
value.) Figures 18 and 19 indicate that, with increasing Mach number and
decreasing altitude, the damping in angle of attack and normal acceler-
ation remain almost unchanged but with a slight tendency towards less
damping. It would appear, therefore, that the reduction in damping
associated with the increasing Mach number as discussed previously tended
to cancel out the improved damping obtained by operation at lower altitudes.

The trend of the amplitude-ratio curves for normal acceleration indi-
cate an increase in magnitude over the entire frequency range as Mach
number was increased and altitude decreased. This trend appears reasonable
for the case where Mach number effects are relatively small because, under
conditions where the stability derivatives do not change appreciably, the
magnitude of the curves increase as a function of the square of the air-
speed when the altitude is held constant. Similarly, for the case of

constant altitude and with no Mach number effects on the stability derivatives, the amplitude ratios in angle of attack would be expected to originate at approximately the same value of static sensitivity and to reach peak values of approximately the same magnitude but would be shifted over the frequency range an amount proportional to airspeed.

These trends are roughly borne out for the test model up to a Mach number of 0.9. Above this Mach number, the over-all reduction of the amplitudes of the frequency response in angle of attack primarily reflects an increase in static stability of the model. The trend is actually greater than indicated since the larger Mach numbers were obtained at lower altitudes and the altitude effect should improve the frequency response. A résumé of altitude effects on the transfer-function coefficients together with their effects on the frequency-response curves is given in reference 15.

The response obtained at a Mach number of 0.725 appears to be somewhat different from those at other subsonic Mach numbers inasmuch as a higher degree of damping and generally lower amplitude ratios are indicated throughout the frequency range investigated. No irregularity was found in the flight records that would tend to dispute or disprove the data obtained at this Mach number.

CONCLUSIONS

As part of a general investigation to obtain the characteristics of airplanes in the transonic-speed range, a model of an airplane configuration having 45° sweptback wing and tail surfaces has been tested by the free-fall technique over a Mach number range of 0.5 to 1.21 in order to determine the lift, drag, and longitudinal stability and control characteristics. The conclusions from these tests are as follows:

1. The configuration experienced only small trim changes in angles of attack and trim lift coefficient in the high subsonic range.

2. The value of the lift-curve slope of the free-fall model increased appreciably with increases in Mach number at subsonic speeds. The lift-curve slope peaked at a Mach number of 0.97 and attained a value 50 percent greater than the value obtained at low subsonic speeds and at a Mach number of 1.2. At transonic speeds, the increase in lift-curve slope with increasing Mach number was much greater than that predicted by the simplified lifting-surface theory.

3. The results of the drag tests indicate near a Mach number of 1.2 that some leading edge suction was realized but that only a moderate percentage of the amount predicted by theory.

4. The ability of the horizontal tail to change the lift coefficient increased with increasing Mach number up to a Mach number of 0.9 and thereafter decreased. At the highest Mach number of the test, the tail was only half as effective in changing the trim lift coefficient as it was at low subsonic speeds. This decrease at supersonic speeds was due to the reduction in lift-curve slope of the tail and to the large increase in static stability of the model.

5. The static stability of the free-fall model decreased slightly with increasing Mach number up to $M = 0.9$, where the aerodynamic center was at 40 percent of the mean aerodynamic chord. As the Mach number was further increased, the static stability increased rapidly until at a Mach number of 1.17 the aerodynamic center was at 70 percent of the mean aerodynamic chord.

6. The longitudinal damping derivative of the model $C_{m_q} + C_{m_{D_\alpha}}$ indicated an increase in damping with increasing Mach number in the subsonic region and a more pronounced decrease in damping with increasing Mach number supersonically. The maximum damping was approximately 50 percent greater than the high- and low-speed values. When the aerodynamic derivatives of the model were used to calculate the dynamic characteristics of a full-size fighter airplane with typical values of center-of-gravity position, moment of inertia in pitch, and wing loading, and flying at an altitude of 30,000 feet, the damping response of the airplane met the handling-qualities specifications at subsonic Mach numbers but required a slightly greater number of cycles to damp to the required amplitude at supersonic Mach numbers.

7. The data calculated from wind-tunnel results for purposes of comparison indicate the same general trends as the free-fall results, the most pronounced difference being in the Mach number at which the large change in the static stability began.

8. The frequency-response curves obtained for the test model show trends typical of swept-wing configurations operating at transonic speeds and, in general, bear out the trends of damping, static sensitivity, and static stability given in conclusions 5 to 7.

Langley Aeronautical Laboratory,
    National Advisory Committee for Aeronautics,
        Langley Field, Va.

REFERENCES

1. Osborne, Robert S.: A Transonic-Wing Investigation in the Langley
      8-Foot High-Speed Tunnel at High Subsonic Mach Numbers and at a
      Mach Number of 1.2. Wing-Fuselage Configuration Having a Wing of
      45° Sweepback, Aspect Ratio 4, Taper Ratio 0.6, and NACA 65A006
      Airfoil Section. NACA RM L50H08, 1950.

2. Osborne, Robert S., and Mugler, John P., Jr.: Aerodynamic Character-
      istics of a 45° Sweptback Wing-Fuselage Combination and the Fuselage
      Alone Obtained in the Langley 8-Foot Transonic Tunnel. NACA
      RM L52E14, 1952.

3. Osborne, Robert S., and Mugler, John P., Jr.: Effects of Wing Elas-
      ticity on the Aerodynamic Characteristics of a 45° Sweptback-Wing-
      Fuselage Combination Measured in the Langley 8-Foot Transonic
      Tunnel. NACA RM L52G23, 1952.

4. Weil, Joseph, and Goodson, Kenneth W.: Aerodynamic Characteristics
      of a Wing With Quarter-Chord Line Swept Back 45°, Aspect Ratio 4,
      Taper Ratio 0.6, and NACA 65A006 Airfoil Section. Transonic-Bump
      Method. NACA RM L9A21, 1949.

5. Kurbjun, Max C., and Thompson, Jim Rogers: Transonic Drag Character-
      istics and Pressure Distribution on the Body of a Wing-Body Combina-
      tion Consisting of a Body of Revolution of Fineness Ratio 12 and a
      Wing Having Sweepback of 45°, Aspect Ratio 4, Taper Ratio 0.6, and
      NACA 65A006 Airfoil Sections. NACA RM L52B12, 1952.

6. Thompson, Jim Rogers: Measurements of the Drag and Pressure Distri-
      bution on a Body of Revolution Throughout Transition From Subsonic
      to Supersonic Speeds. NACA RM L9J27, 1950.

7. Phillips, William H.: Effect of Steady Rolling on Longitudinal and
      Directional Stability. NACA TN 1627, 1948.

8. Mathews, Charles W., and Kurbjun, Max C.: An Analysis of the Factors
      Affecting the Loss in Lift and Shift in Aerodynamic Center Produced
      by the Distortion of a Swept Wing Under Aerodynamic Load. NACA
      TN 2901, 1953.

9. Diederich, Franklin W., and Foss, Kenneth A.: Charts and Approximate
      Formulas for the Estimation of Aeroelastic Effects on the Loading
      of Swept and Unswept Wings. NACA TN 2608, 1952.

10. Greenberg, Harry: A Survey of Methods for Determining Stability
      Parameters of an Airplane From Dynamic Flight Measurements. NACA
      TN 2340, 1951.

11. DeYoung, John, and Harper, Charles W.: Theoretical Symmetric Span
      Loading at Subsonic Speeds for Wings Having Arbitrary Plan Form.
      NACA Rep. 921, 1948.

12. Jones, Robert T.: Estimated Lift-Drag Ratios at Supersonic Speed.
      NACA TN 1350, 1947.

13. Anon.: Specification for Flying Qualities of Piloted Airplanes.
      NAVAER SR-119B, Bur. Aero., June 1, 1948.

14. Stokes, Fred H., and Matthews, J. T.: Theoretical Investigation
      of the Longitudinal Response Characteristics of a Swept-Wing
      Fighter Airplane Having a Pitch-Attitude Control System. NACA
      TN 2882, 1953.

15. Triplett, William C., and Smith, G. Allan: Longitudinal Frequency-
      Response Characteristics of a 35° Swept-Wing Airplane As Determined
      From Flight Measurements, Including a Method for the Evaluation of
      Transfer Functions. NACA RM A51G27, 1951.

TABLE I

COORDINATES OF THE FINENESS-RATIO-10 BODY

X, in.	Y, in.	X, in.	Y, in.
0	0	48.00	4.876
.60	.277	54.00	4.971
.90	.358	60.00	5.000
1.50	.514	66.00	4.955
3.00	.866	72.00	4.828
6.00	1.446	78.00	4.610
9.00	1.936	84.00	4.274
12.00	2.365	90.00	3.754
18.00	3.112	96.00	3.031
24.00	3.708	100.00	2.485
30.00	4.158		
36.00	4.489		
42.00	4.719		

██████████L

TABLE II

TRANSFER FUNCTIONS

$$\frac{\alpha}{i_t} = \frac{\left[\dfrac{-c_{L_{i_t}}}{2\mu}\right]D + \left[\dfrac{c_{L_{i_t}}c_{m_q} + 4\mu c_{m_{i_t}}}{8\mu^2 K_y^2}\right]}{D^2 + \left[\dfrac{2K_y^2 c_{L_\alpha} - c_{m_q} - c_{m_{D\alpha}}}{4\mu K_y^2}\right]D + \left[\dfrac{-c_{m_q}c_{L_\alpha} - 4\mu c_{m_\alpha}}{8\mu^2 K_y^2}\right]}$$

$$\frac{n}{i_t} = \frac{V^2}{g\bar{c}} \cdot \frac{\left[\dfrac{c_{L_{i_t}}}{2\mu}\right]D^2 + \left[\dfrac{-c_{L_{i_t}}\left(c_{m_{D\alpha}} + c_{m_q}\right)}{8\mu^2 K_y^2}\right]D + \left[\dfrac{c_{L_\alpha}c_{m_{i_t}} - c_{m_\alpha}c_{L_{i_t}}}{4\mu^2 K_y^2}\right]}{D^2 + \left[\dfrac{2K_y^2 c_{L_\alpha} - c_{m_q} - c_{m_{D\alpha}}}{4\mu K_y^2}\right]D + \left[\dfrac{-c_{m_q}c_{L_\alpha} - 4\mu c_{m_\alpha}}{8\mu^2 K_y^2}\right]}$$

Mach number	Altitude, ft	α/i_t, deg/deg	n/i_t, g/deg
0.725	32,000	$\dfrac{-4.8537s + 80.547}{s^2 + 2.08s + 49.209}$	$\dfrac{-0.0599s^2 - 0.02866s + 8.853}{s^2 + 2.08s + 49.209}$
.775	30,500	$\dfrac{-7.1320s + 90.672}{s^2 + 1.25s + 62.40}$	$\dfrac{-0.04675s^2 - 0.22644s + 18.565}{s^2 + 1.25s + 62.40}$
.840	28,500	$\dfrac{-1.7597s + 113.834}{s^2 + 1.823s + 79.69}$	$\dfrac{-0.03723s^2 - 0.67041s + 28.048}{s^2 + 1.823s + 79.69}$
.890	27,000	$\dfrac{-1.9125s + 193.996}{s^2 + 2.32s + 99.99}$	$\dfrac{-0.04130s^2 - 0.12528s + 46.035}{s^2 + 2.32s + 99.99}$
.950	25,500	$\dfrac{-0.141s + 174.872}{s^2 + 2.55s + 161.92}$	$\dfrac{-0.0636s^2 + 0.8400s + 60.920}{s^2 + 2.55s + 161.92}$
1.040	22,000	$\dfrac{-0.990s + 387.08}{s^2 + 4.00s + 371.0}$	$\dfrac{-0.11546s^2 - 1.3350s + 159.021}{s^2 + 4.00s + 371.0}$
1.170	15,200	$\dfrac{3.1517s + 513.56}{s^2 + 4.30s + 535.5}$	$\dfrac{-0.1767s^2 + 0.3169s + 261.970}{s^2 + 4.30s + 535.5}$

<NACA>
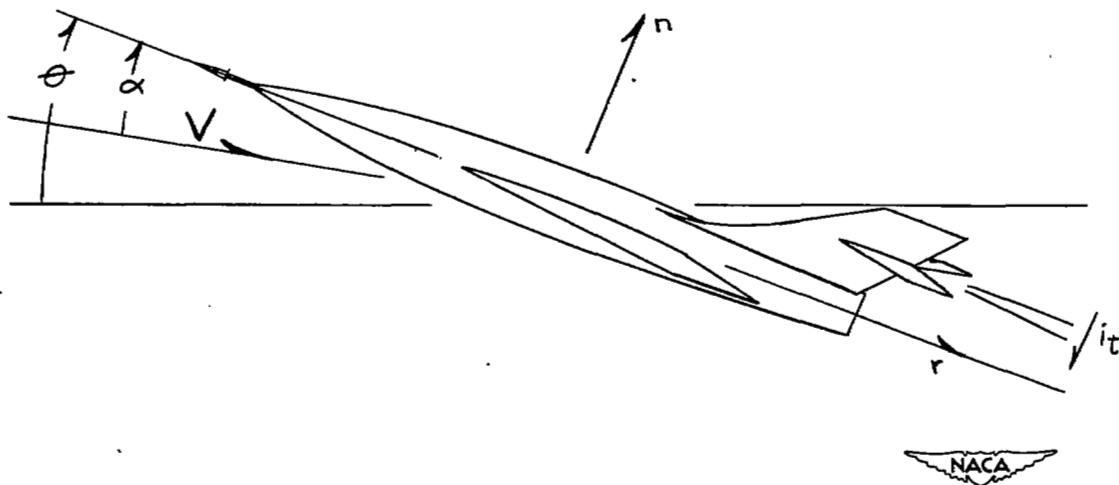
Figure 1.- Sketch of system of axes used in this report with positive
directions and deflections indicated.
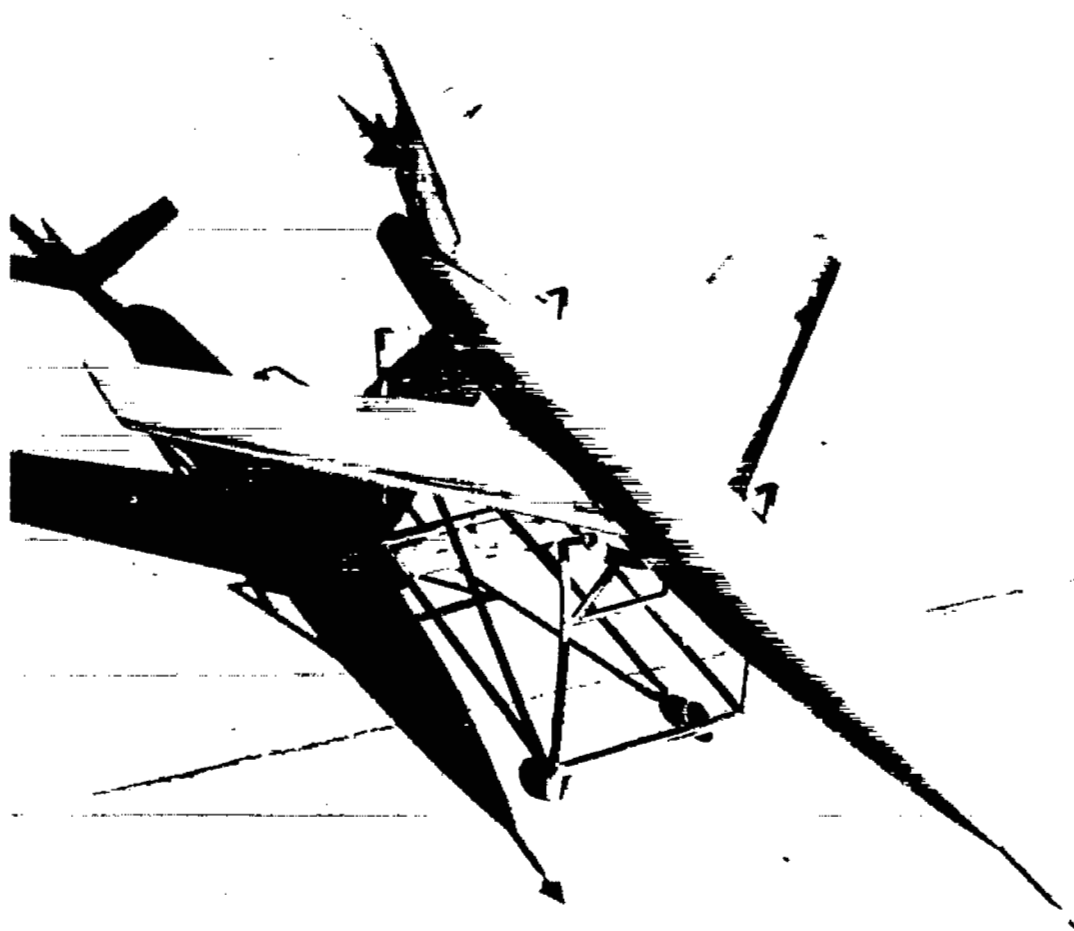
Figure 2.- Photograph of complete model.

Figure 3.- Details and dimensions of complete model. Coordinates of body
surface are given in table I. Dimensions are in inches or as noted.
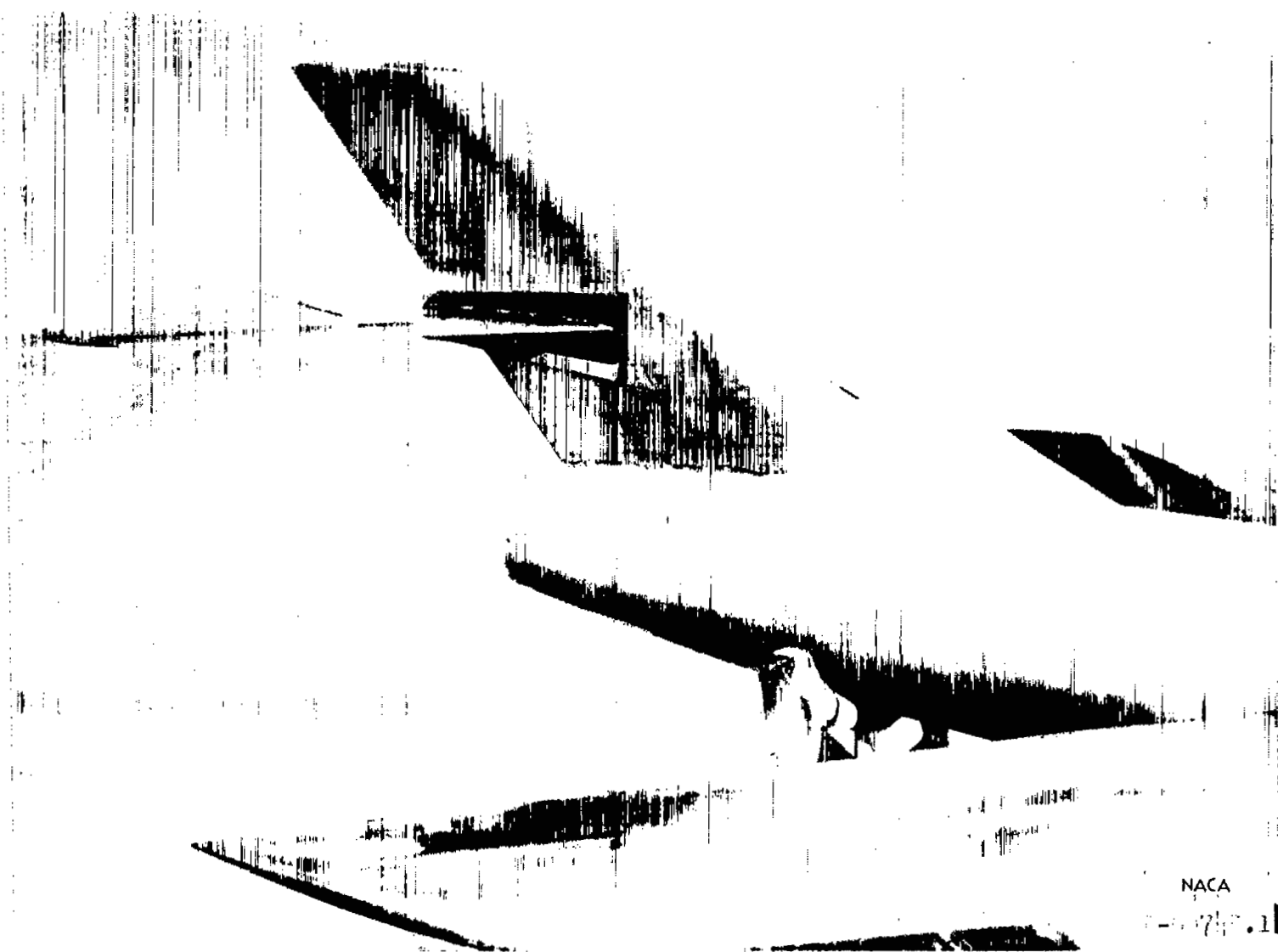
Figure 4.- Photograph of horizontal and vertical tails.

L-69744
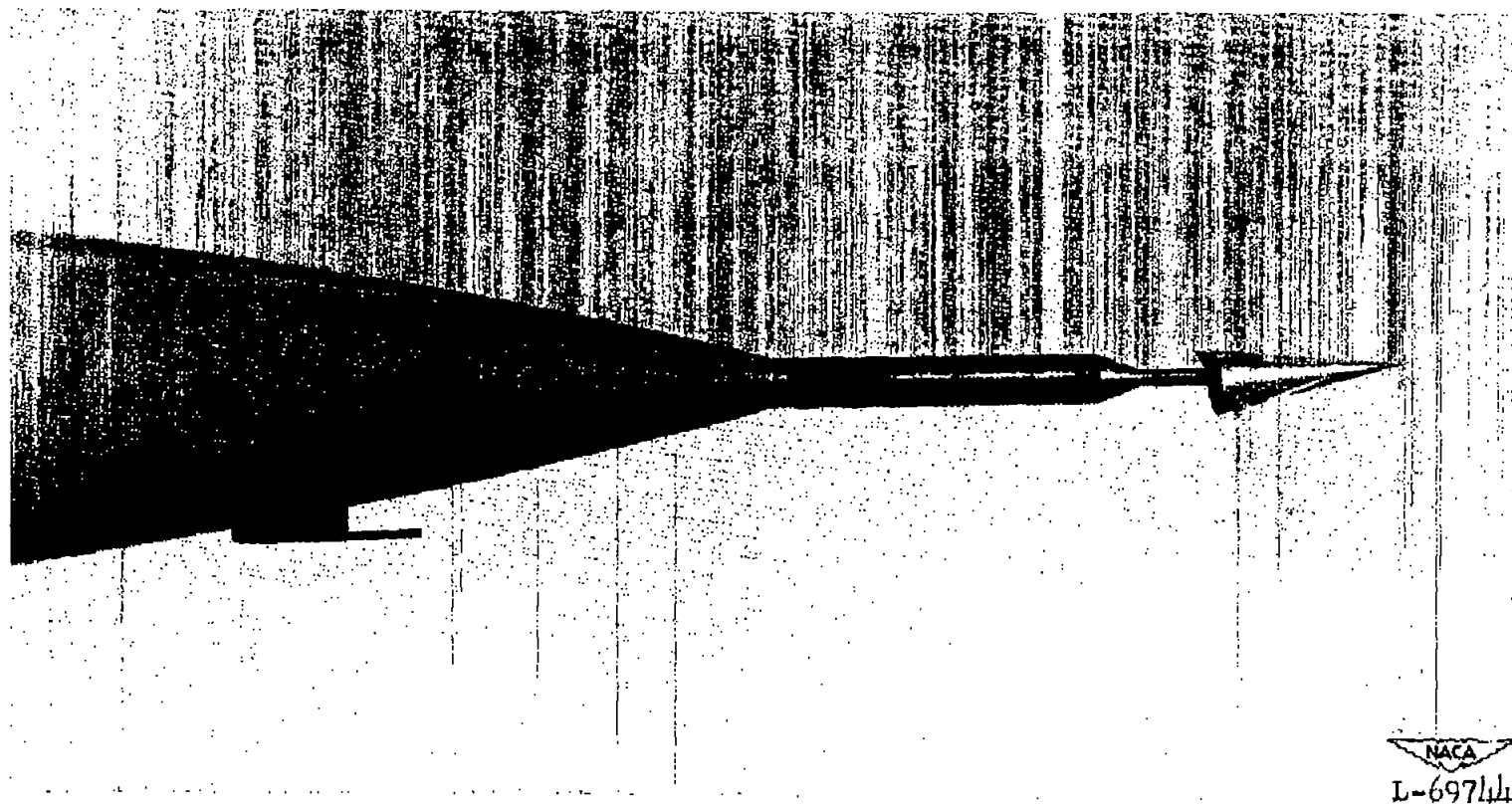
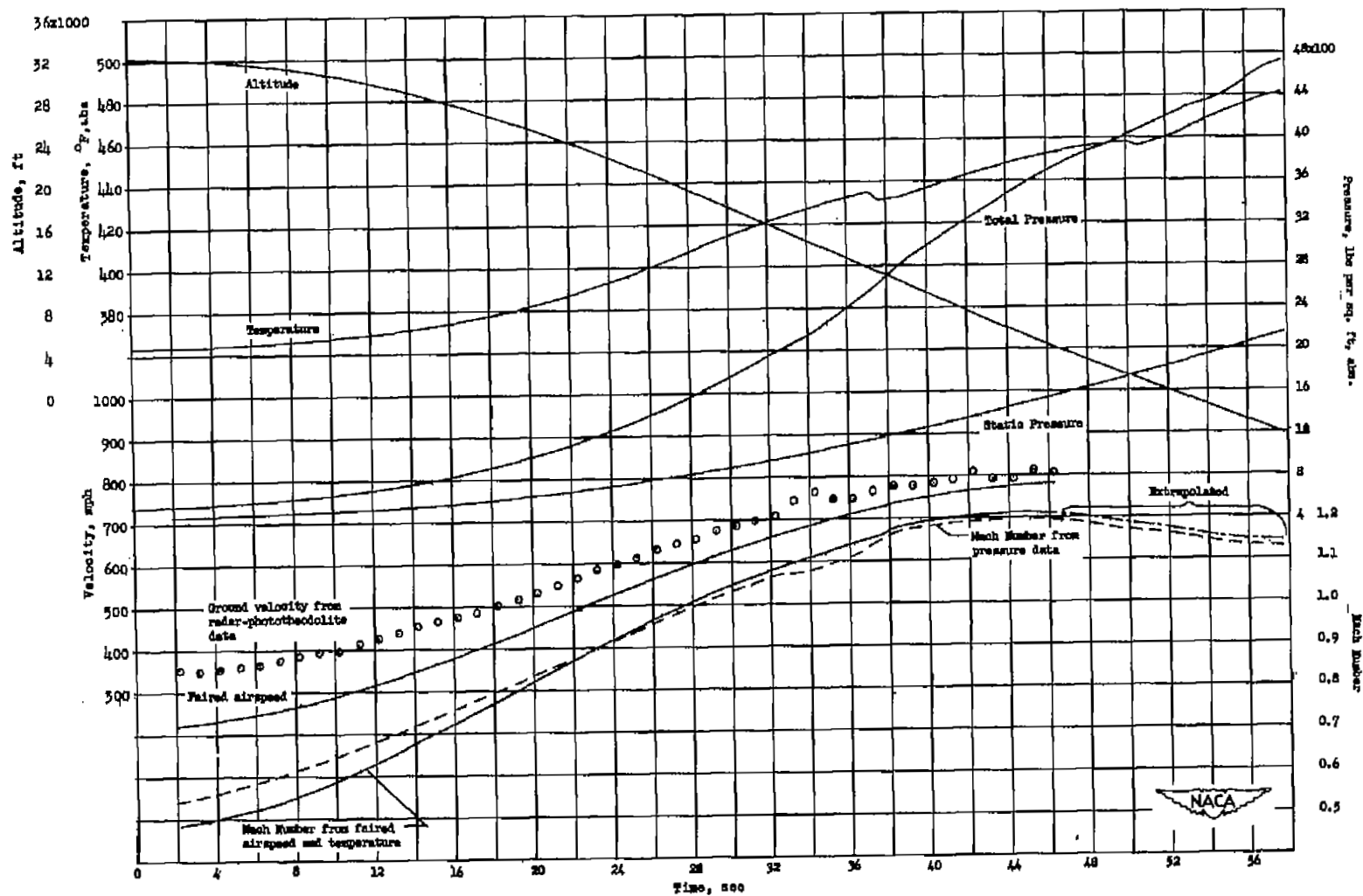Figure 5.- Photograph of angle-of-attack vane and total head pressure pickup.
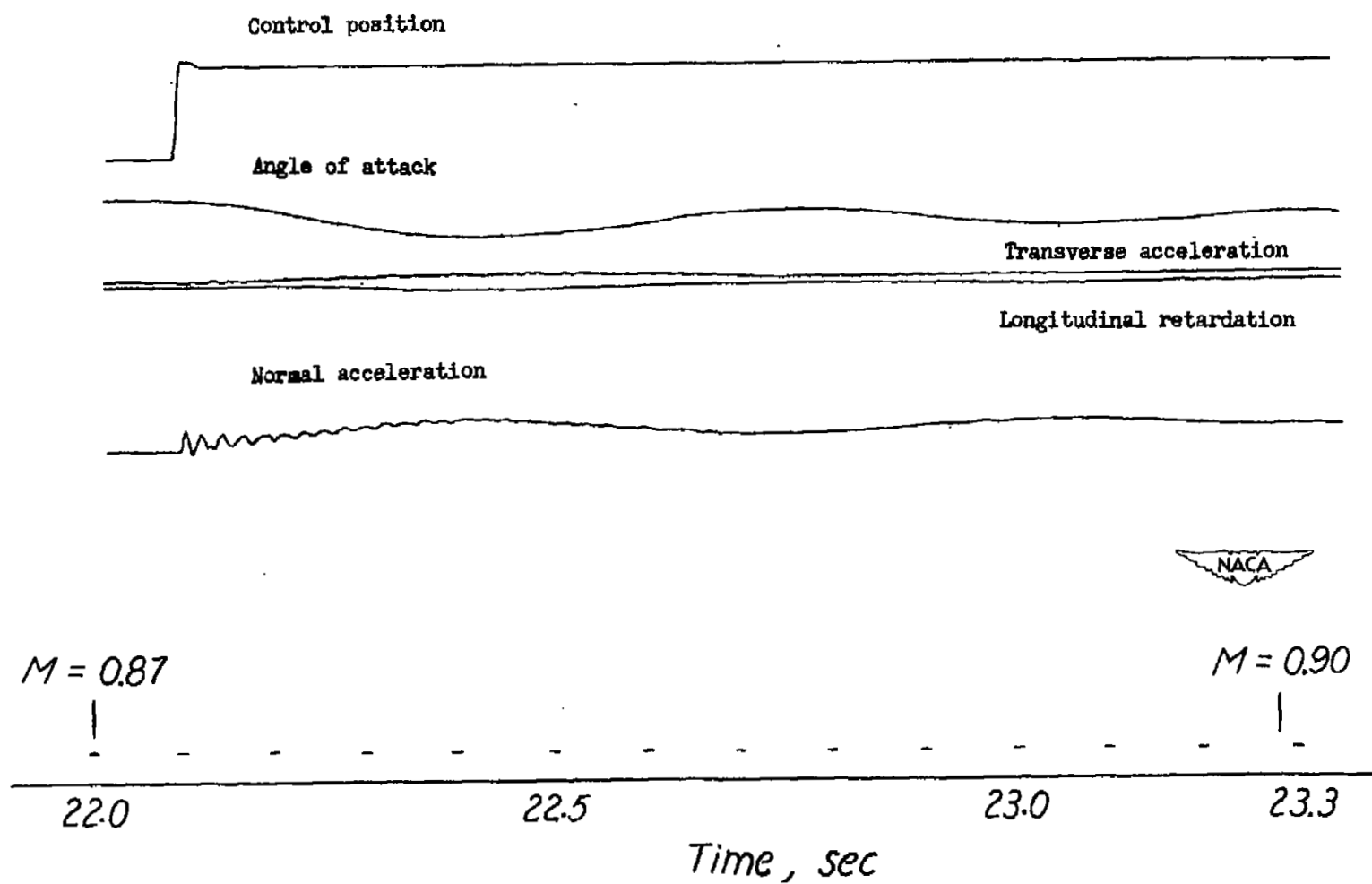
Figure 6.- Quantities used to determine Mach number.

Control position

Angle of attack

Transverse acceleration

Longitudinal retardation

Normal acceleration

NACA

$M = 0.87$

$M = 0.90$

22.0   22.5   23.0   23.3

Time, sec

Figure 7.- Full-size reproduction of a section of the record film.
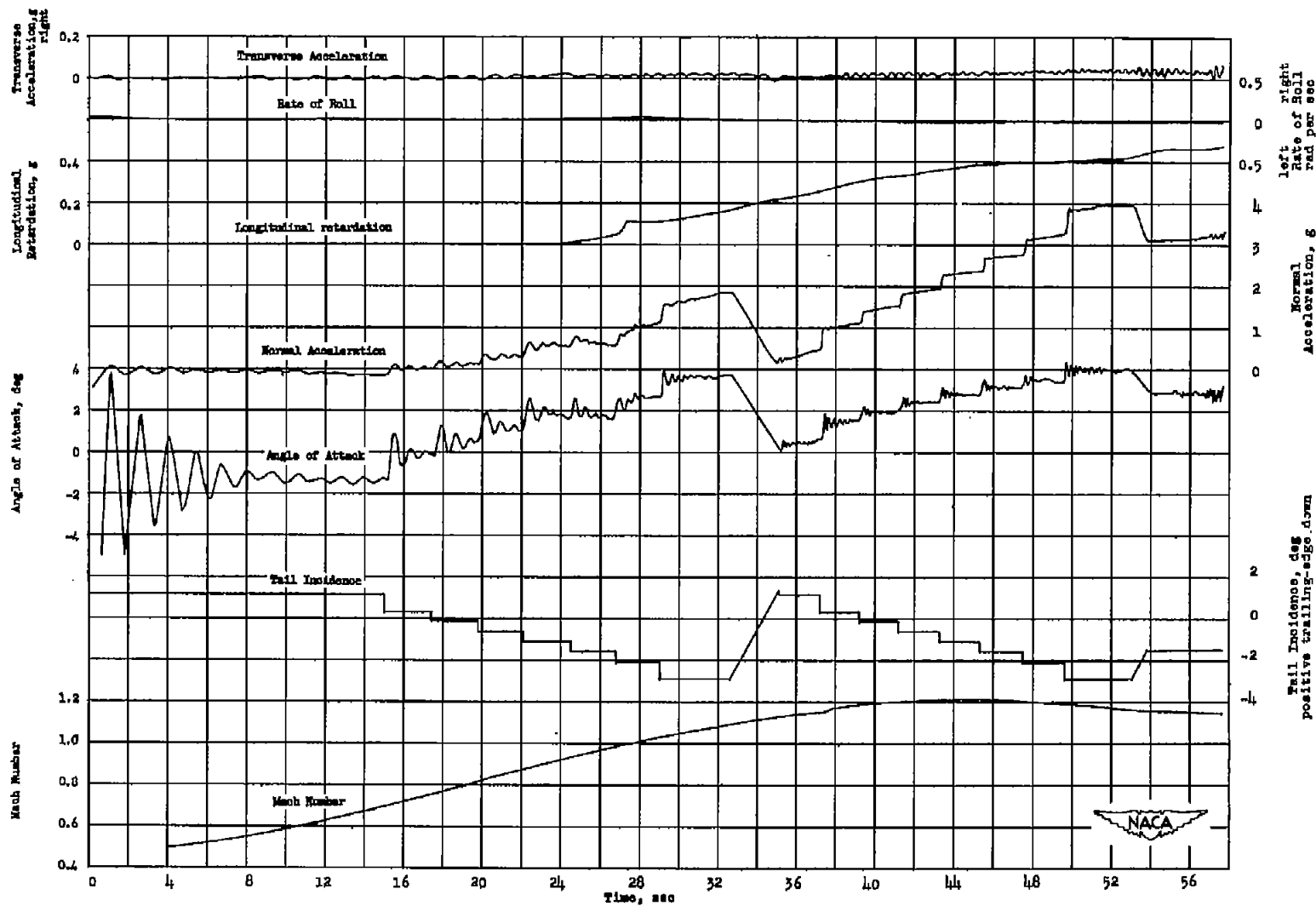
Figure 8.- Time histories of recorded data.
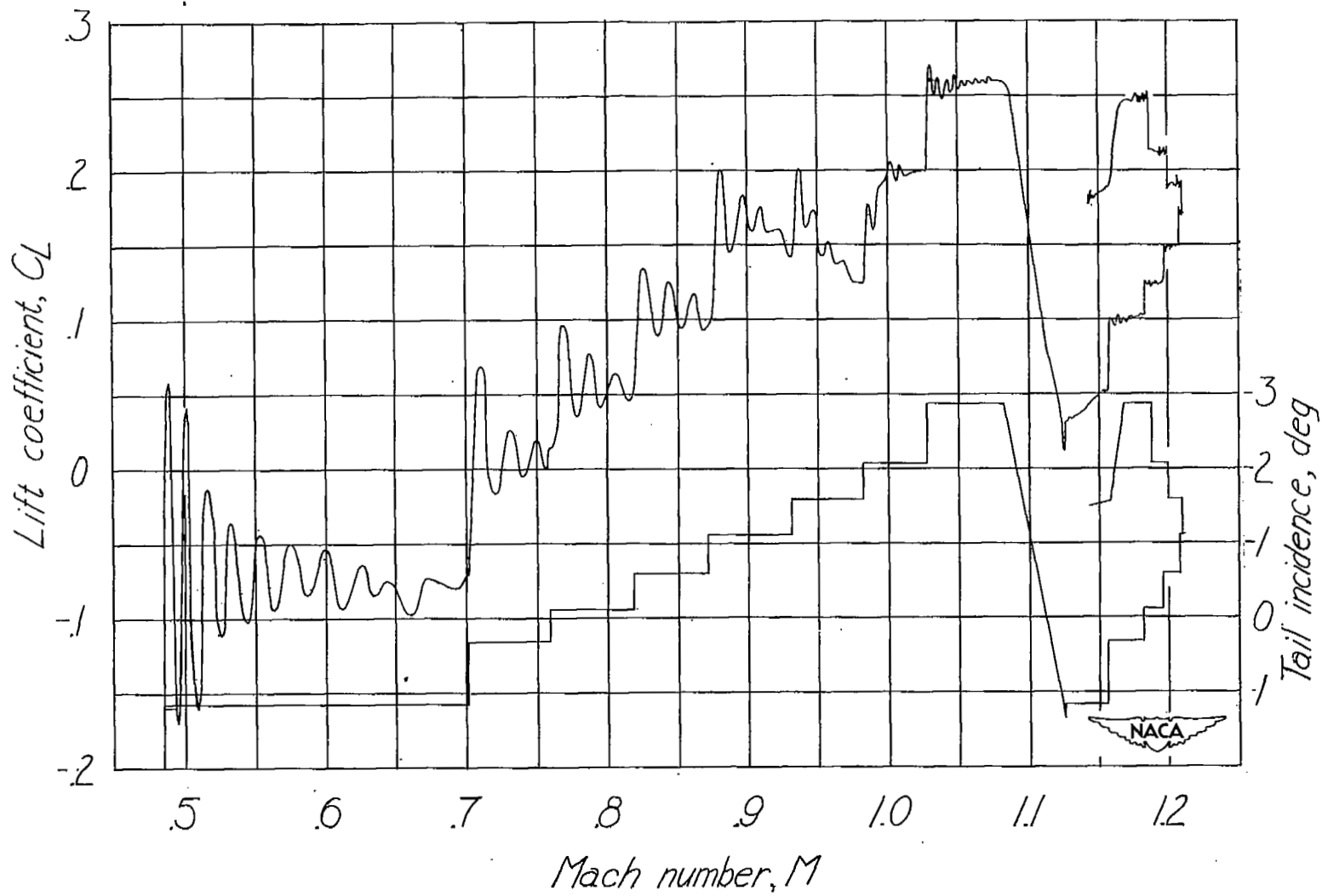
Figure 9.- Variation of model lift coefficient with Mach number.
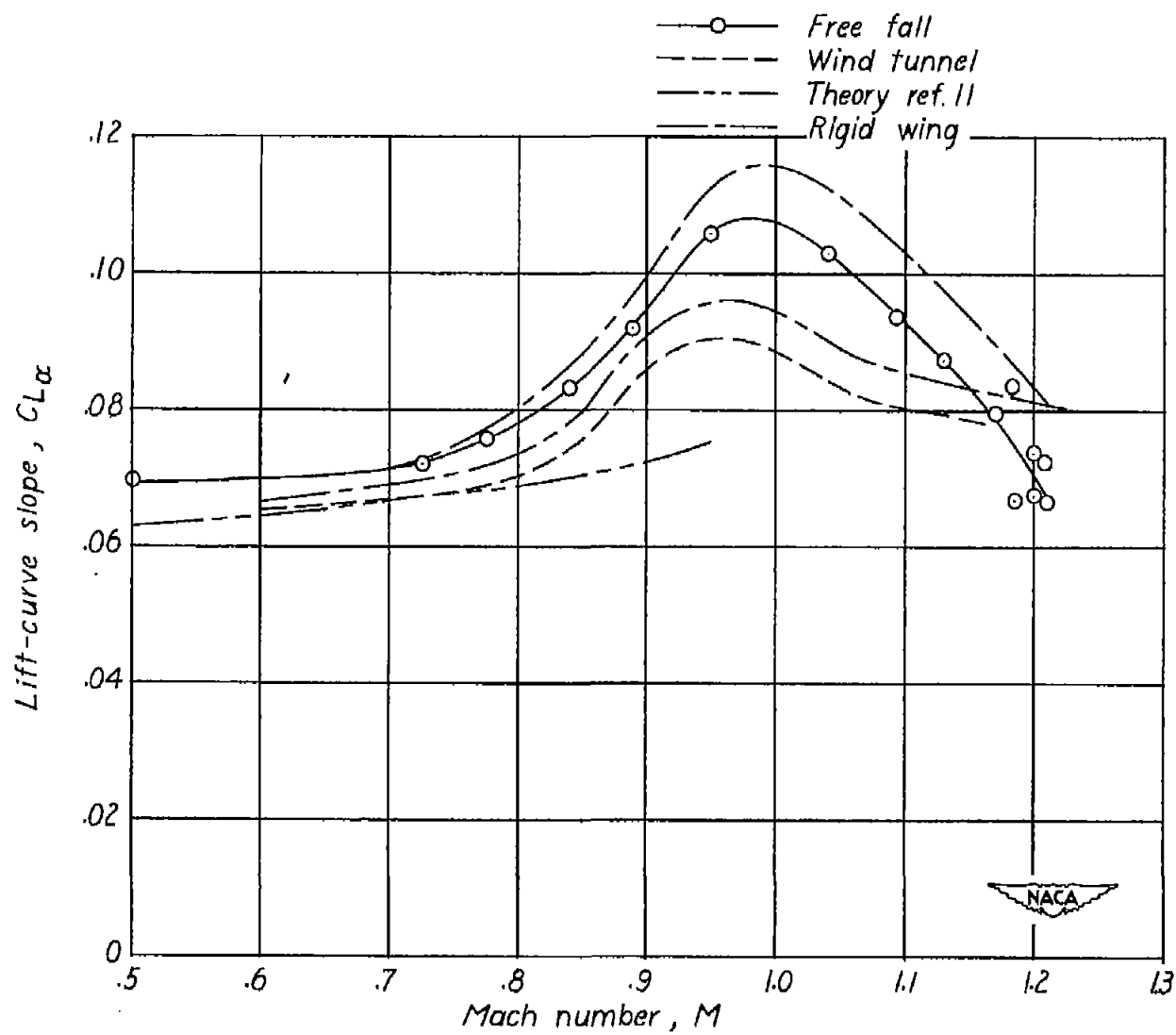
Figure 10.- Variation of the lift-curve slope with Mach number.
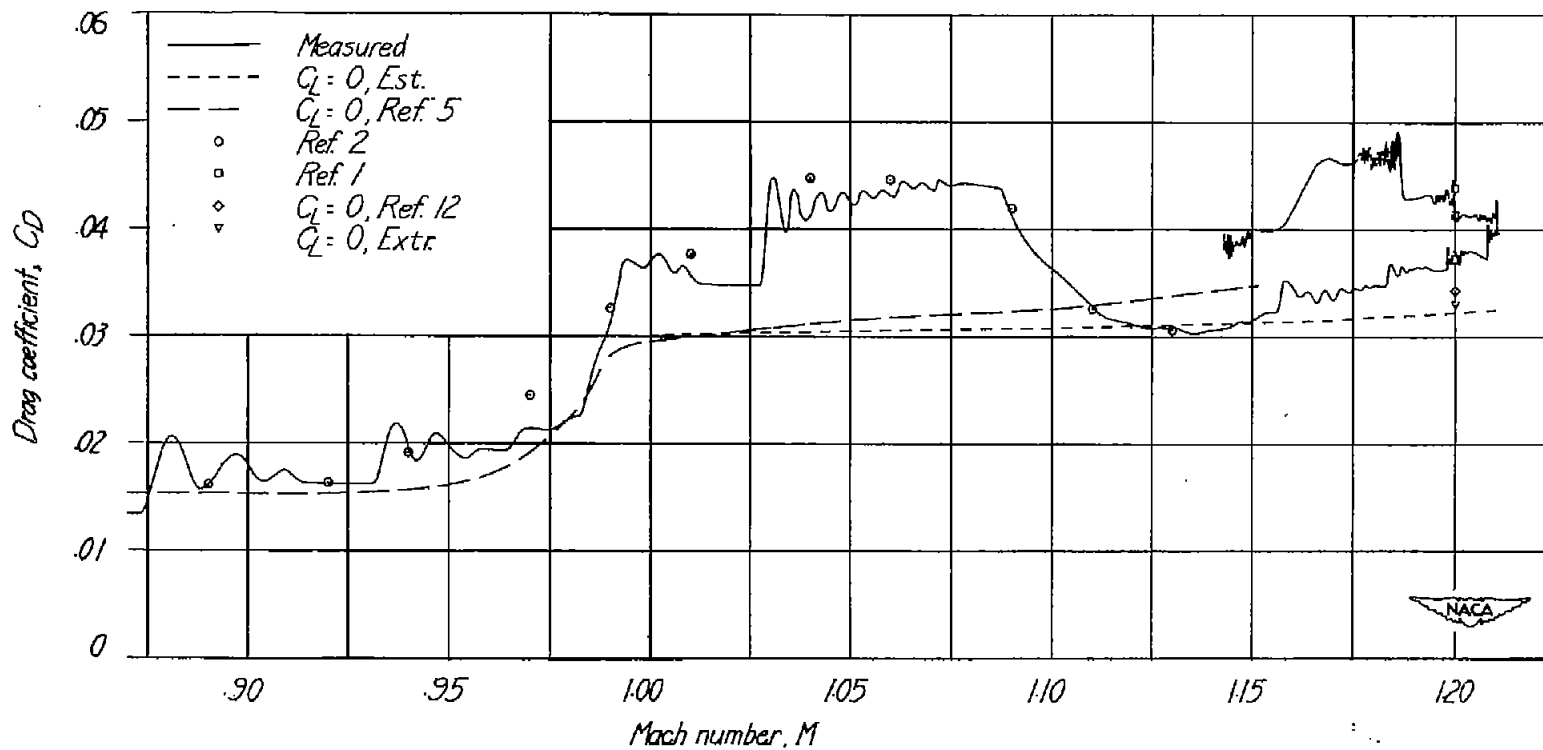
Figure 11.- Variation of drag coefficient with Mach number.
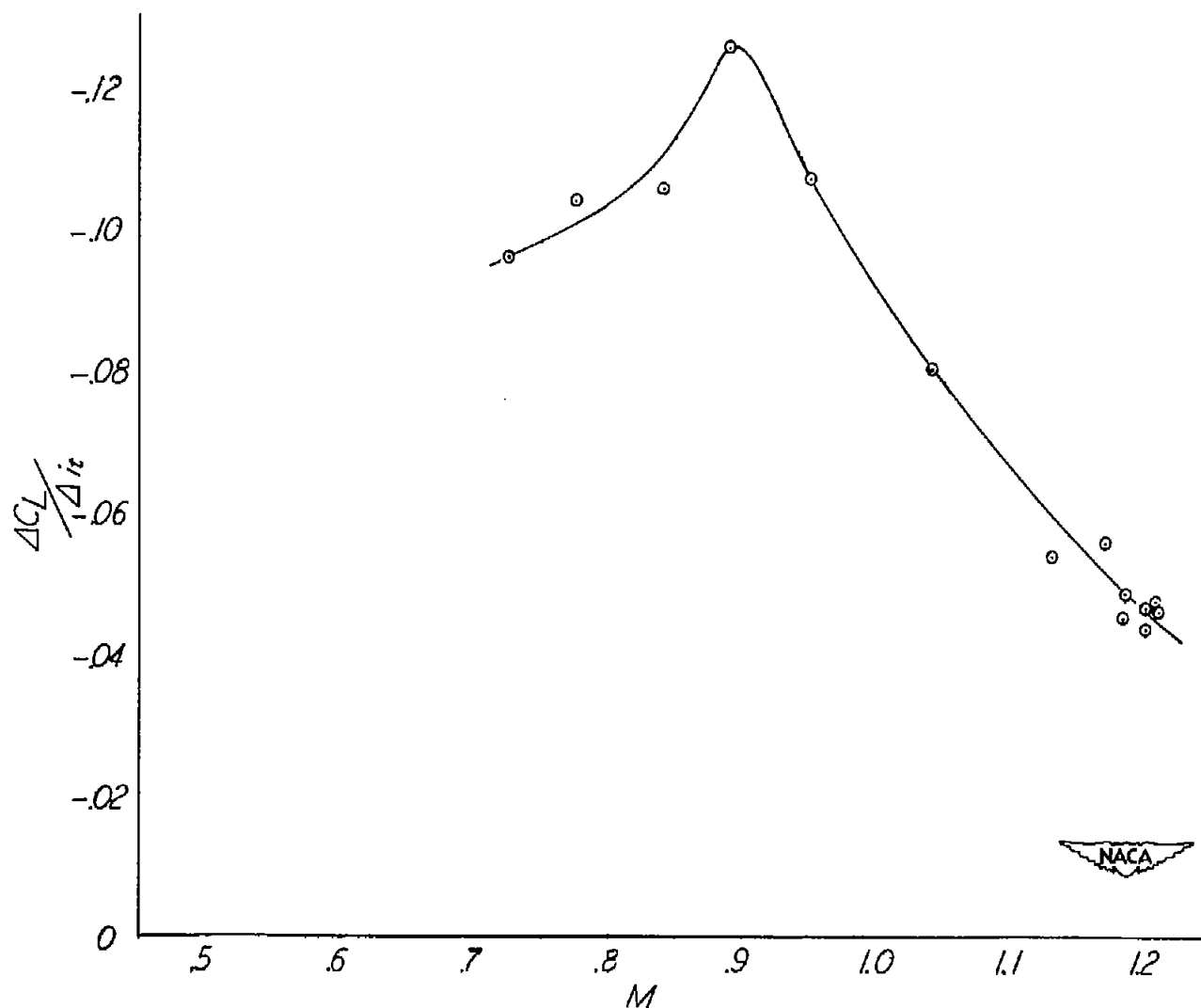
Figure 12.- Variation with Mach number of the ability of the horizontal tail to change the model lift coefficient.
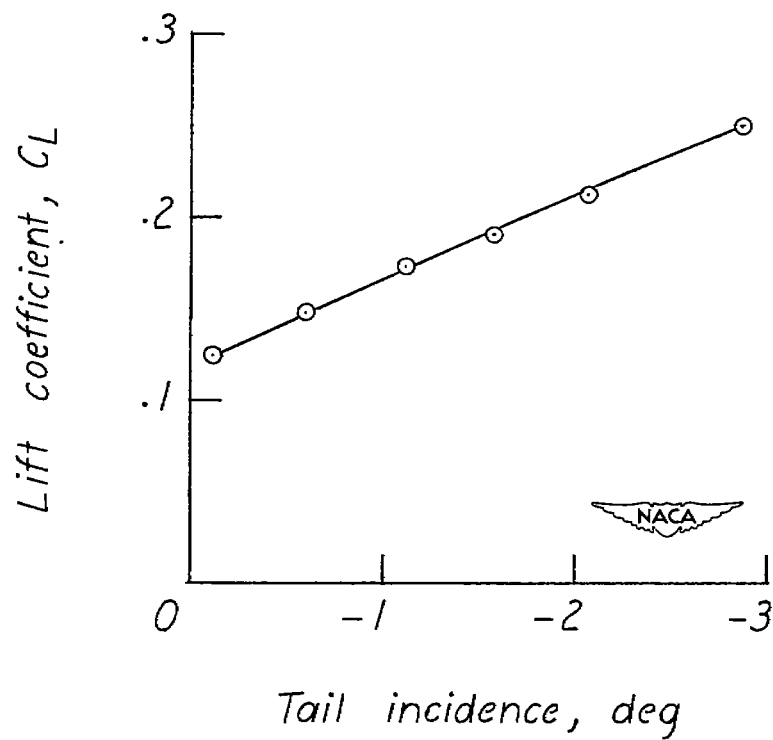
Figure 13.- Variation of the lift coefficient with tail-incidence angle at Mach numbers near 1.2.
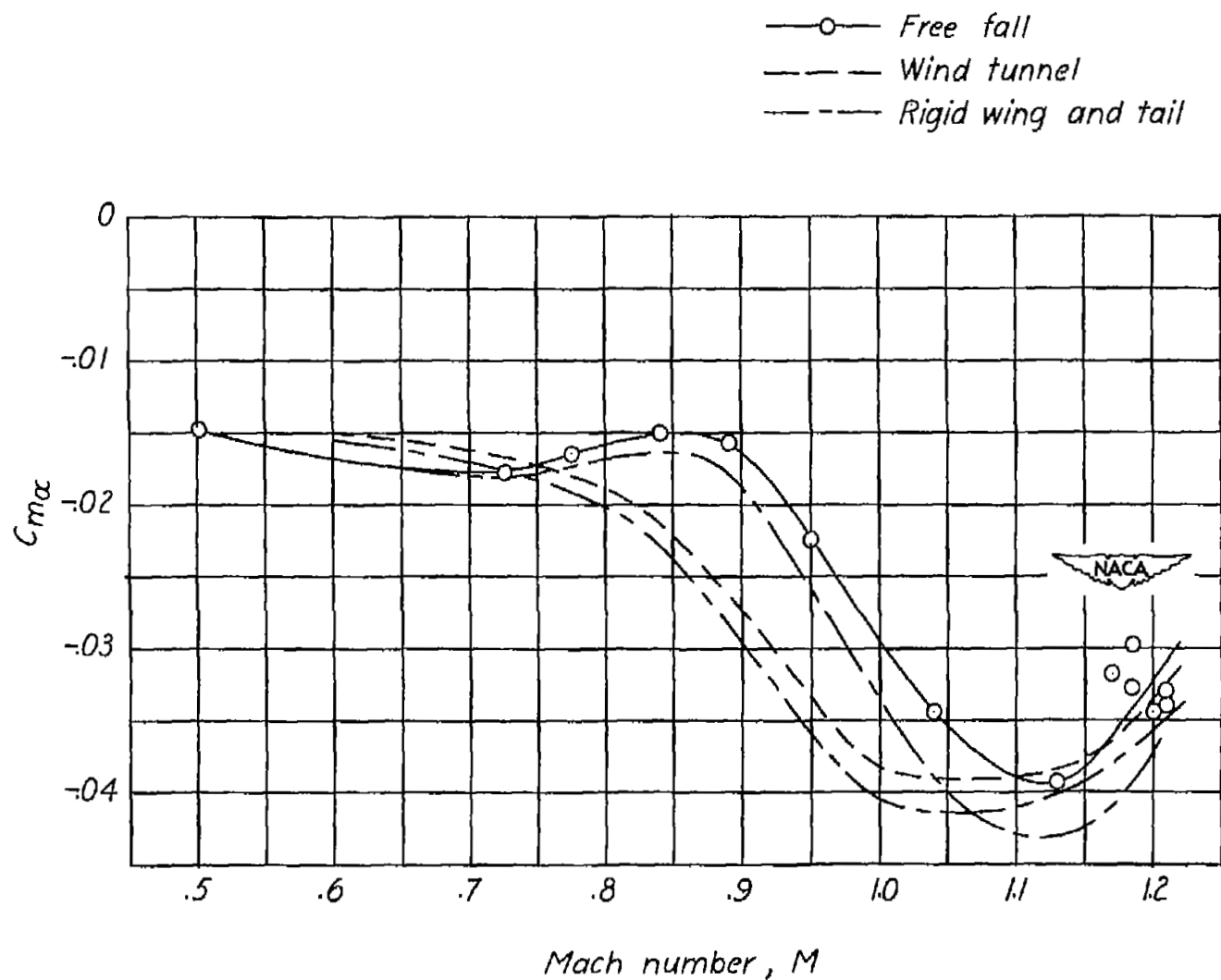
Figure 14.- Variation of the static longitudinal stability derivative C_{m_α} with Mach number. Center of gravity located at 23.64 percent $\bar{c}$.
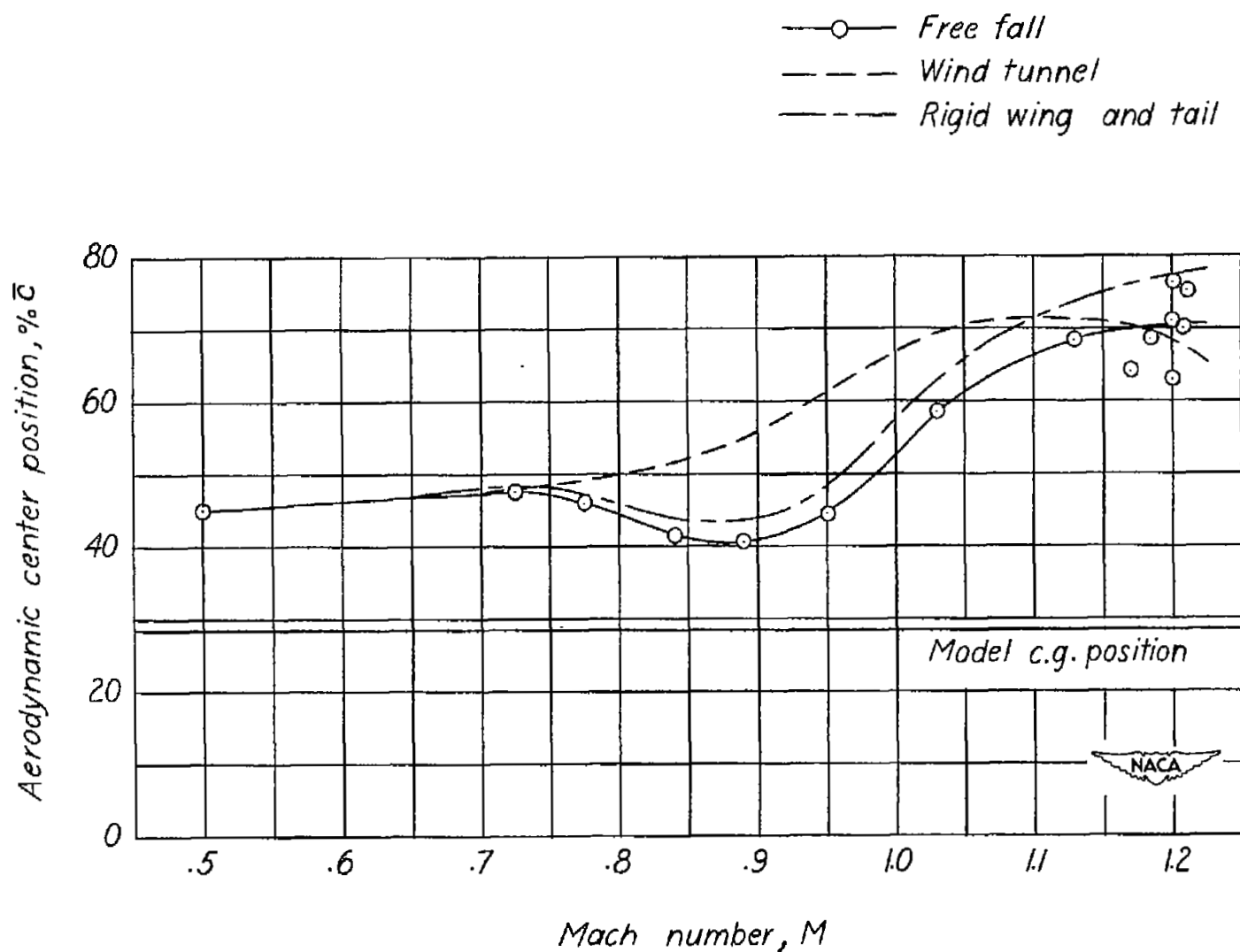
Figure 15.- Variation of the aerodynamic-center position of complete configuration with Mach number.
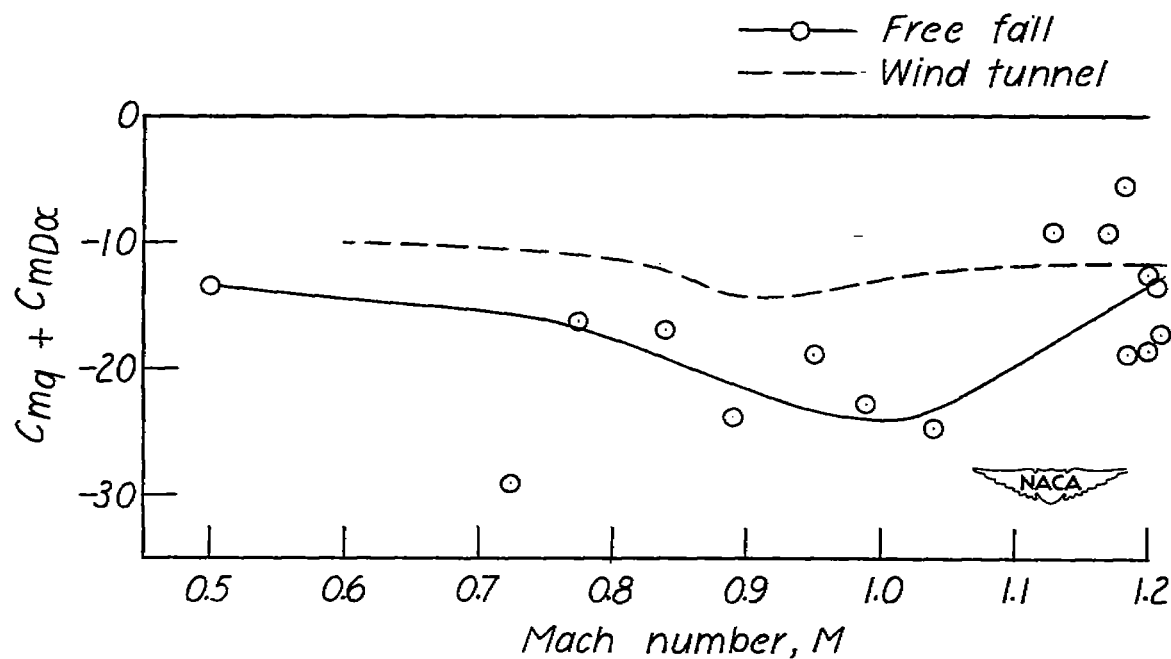
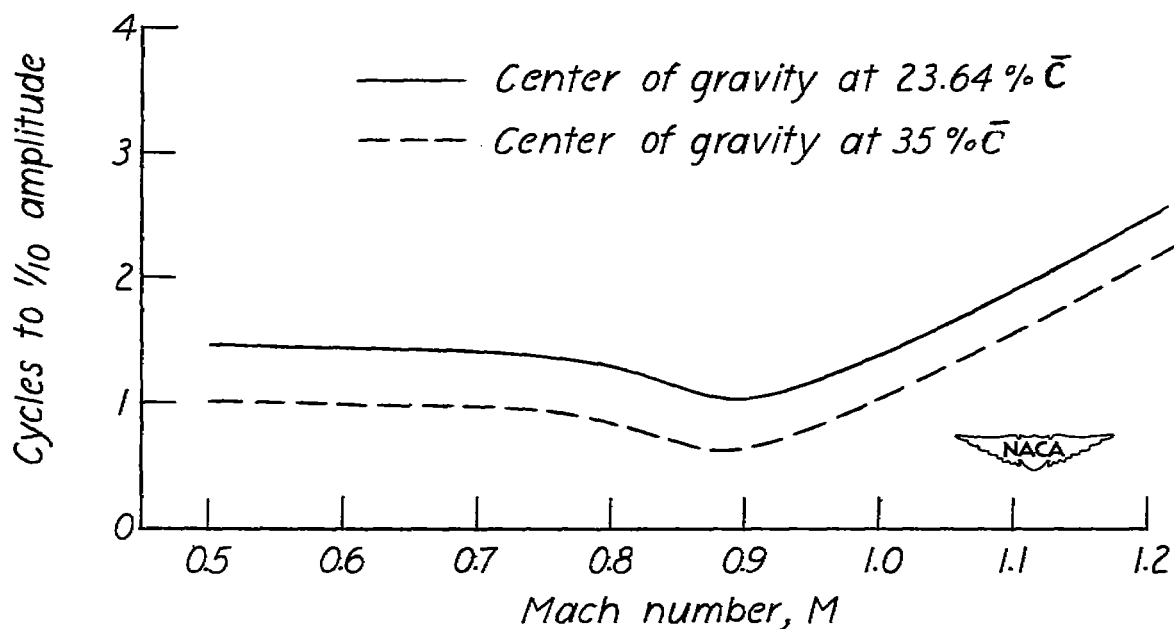Figure 16.- Variation with Mach number of the damping derivative $C_{m_q} + C_{m_{D_\alpha}}$.

Figure 17.- Variation with Mach number of the number of cycles required for the pitch oscillation to damp to 1/10 amplitude for an airplane of fighter size and weight flying at 30,000 feet.
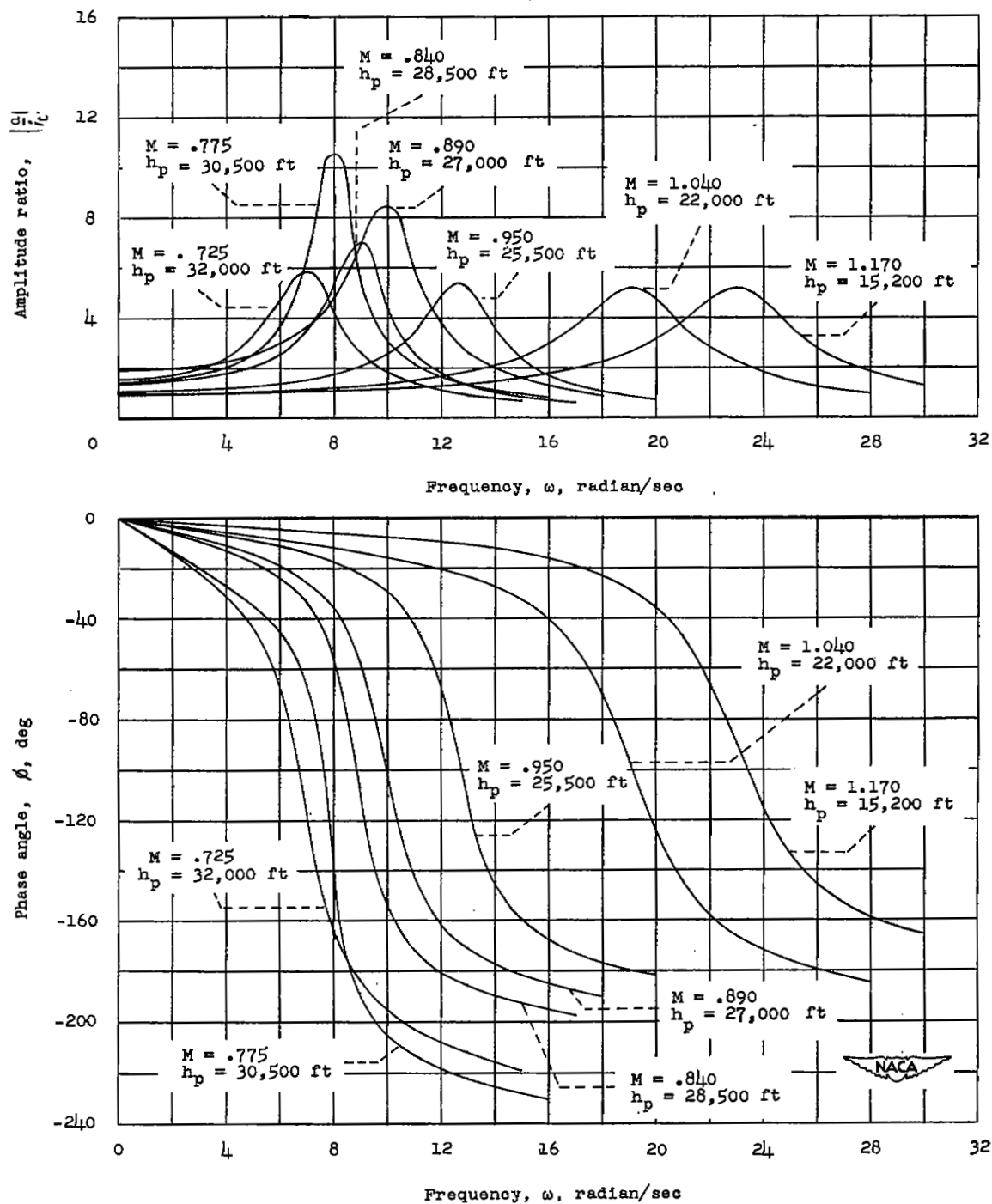
Figure 18.- Frequency-response data for the response of the angle of attack
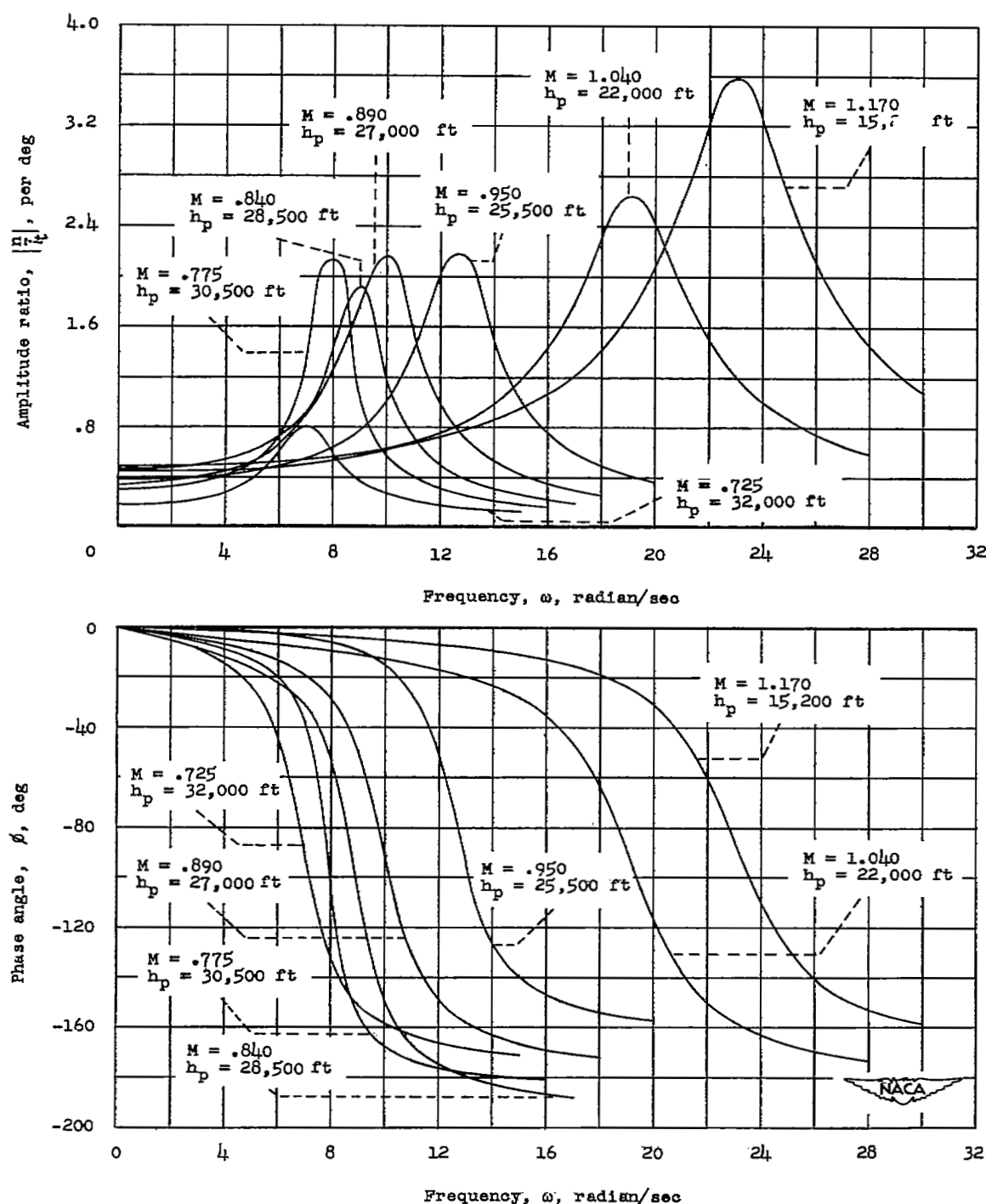to the step elevator deflection.

Figure 19.- Frequency-response data for the response of the normal
acceleration to the step elevator deflection.